

Bubble Shapes and Terminal Velocities

Having introduced the Haberman-Morton number, we can now identify the conditions for departure from sphericity. For low Reynolds numbers ($Re \ll 1$) the terminal velocity will be given by $Re \propto Fr^2$. Then the shape will deviate from spherical when $We \geq Re$ or, using $Re \propto Fr^2$ and $Hm = We^3 Fr^{-2} Re^{-4}$, when

$$Re \geq Hm^{-\frac{1}{2}} \quad (\text{Nfc1})$$

Thus if $Hm < 1$ all bubbles for which $Re \ll 1$ will remain spherical. However, there are some unusual circumstances in which $Hm > 1$ and then there will be a range of Re , namely $Hm^{-\frac{1}{2}} < Re < 1$, in which significant departure from sphericity might occur.

For high Reynolds numbers ($Re \gg 1$) the terminal velocity is given by $Fr \approx O(1)$ and distortion will occur if $We > 1$. Using $Fr = 1$ and $Hm = We^3 Fr^{-2} Re^{-4}$ it follows that departure from sphericity will occur when

$$Re \gg Hm^{-\frac{1}{4}} \quad (\text{Nfc2})$$

Consequently, in the common circumstances in which $Hm < 1$, there exists a range of Reynolds numbers, $Re < Hm^{-\frac{1}{4}}$, in which sphericity is maintained; nonspherical shapes occur when $Re > Hm^{-\frac{1}{4}}$. For $Hm > 1$ departure from sphericity has already occurred at $Re < 1$ as discussed above.

Experimentally, it is observed that the initial departure from sphericity causes ellipsoidal bubbles that may oscillate in shape and have oscillatory trajectories (Hartunian and Sears 1957). As the bubble size is further increased to the point at which $We \approx 20$, the bubble acquires a new asymptotic shape, known as a *spherical-cap bubble*. A photograph of a typical spherical-cap bubble is shown in figure 1; the notation used to describe the approximate geometry of these bubbles is sketched in the same figure. Spherical-cap bubbles were first investigated by Davies and Taylor (1950), who observed that the terminal velocity is simply related to the radius of curvature of the cap, R_C , or to the equivalent volumetric radius, R_B , by

$$W_\infty = \frac{2}{3}(gR_C)^{\frac{1}{2}} = (gR_B)^{\frac{1}{2}} \quad (\text{Nfc3})$$

Assuming a typical laminar drag coefficient of $C_D = 0.5$, a spherical solid particle with the same volume would have a terminal velocity,

$$W_\infty = (8gR_B/3C_D)^{\frac{1}{2}} = 2.3(gR_B)^{\frac{1}{2}} \quad (\text{Nfc4})$$

that is substantially higher than the spherical-cap bubble. From equation (Nfc3) it follows that the effective C_D for spherical-cap bubbles is 2.67 based on the area πR_B^2 .

Wegener and Parlange (1973) have reviewed the literature on spherical-cap bubbles. Figure 2 is taken from their review and shows that the value of $W_\infty/(gR_B)^{\frac{1}{2}}$ reaches a value of about 1 at a Reynolds number, $Re = 2W_\infty R_B/\nu_L$, of about 200 and, thereafter, remains fairly constant. Visualization of the flow reveals that, for Reynolds numbers less than about 360, the wake behind the bubble is laminar and takes the form of a toroidal vortex (similar to a Hill (1894) spherical vortex) shown in the left-hand photograph of figure 3. The wake undergoes transition to turbulence about $Re = 360$, and bubbles at higher Re have turbulent wakes as illustrated in the right side of figure 3. We should add that scuba divers have long observed that spherical-cap bubbles rising in the ocean seem to have a maximum size of the order of 30 cm in diameter. When they grow larger than this, they fission into two (or more) bubbles. However, the author has found no quantitative study of this fission process.

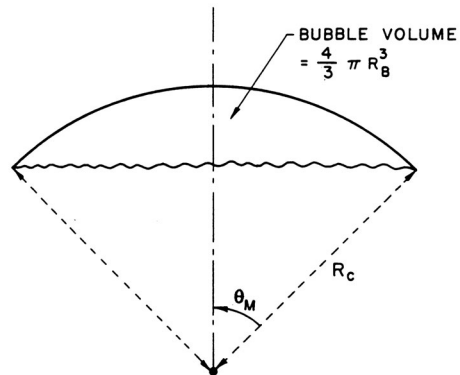
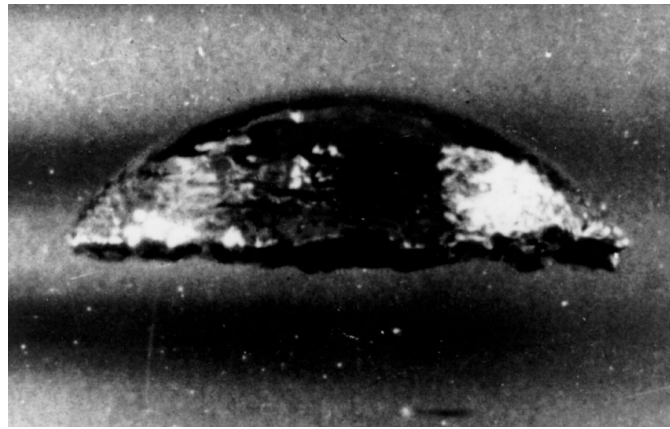


Figure 1: Photograph of a spherical cap bubble rising in water (from Davenport, Bradshaw, and Richardson 1967) with the notation used to describe the geometry of spherical cap bubbles.

In closing, we note that the terminal velocities of the bubbles discussed here may be represented according to the functional relation of equations (Nfb3) as a family of $C_D(Re)$ curves for various Hm . Figure 4 has been extracted from the experimental data of Haberman and Morton (1953) and shows the dependence of $C_D(Re)$ on Hm at intermediate Re . The curves cover the spectrum from the low Re spherical bubbles to the high Re spherical cap bubbles. The data demonstrate that, at higher values of Hm , the drag coefficient makes a relatively smooth transition from the low Reynolds number result to the spherical cap value of about 2.7. Lower values of Hm result in a deep minimum in the drag coefficient around a Reynolds number of about 200.

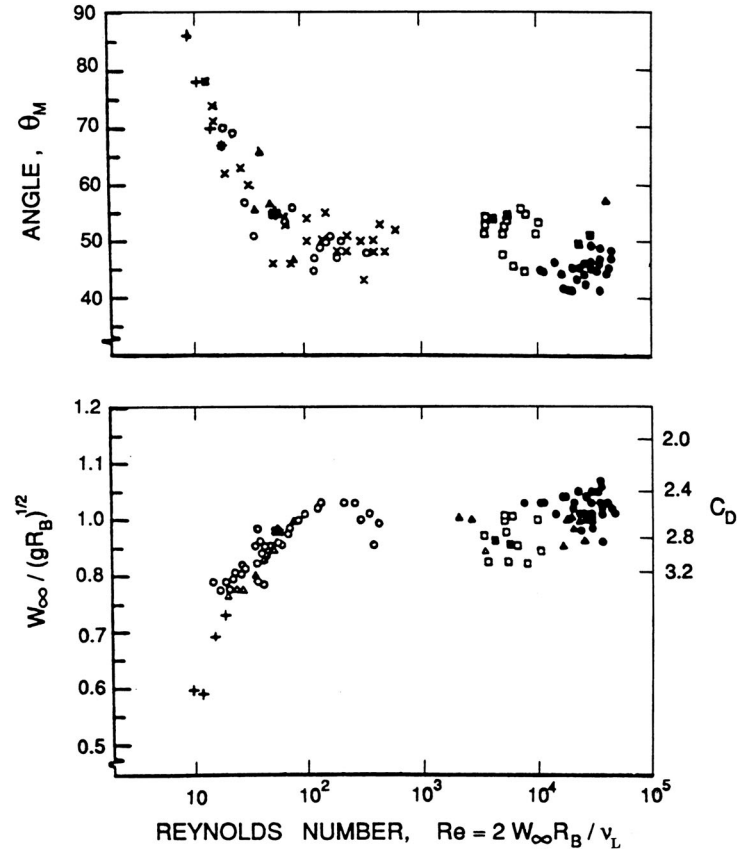


Figure 2: Data on the terminal velocity, $W_\infty/(gR_B)^{1/2}$, and the conical angle, θ_M , for spherical-cap bubbles studied by a number of different investigators (adapted from Wegener and Parlange 1973).

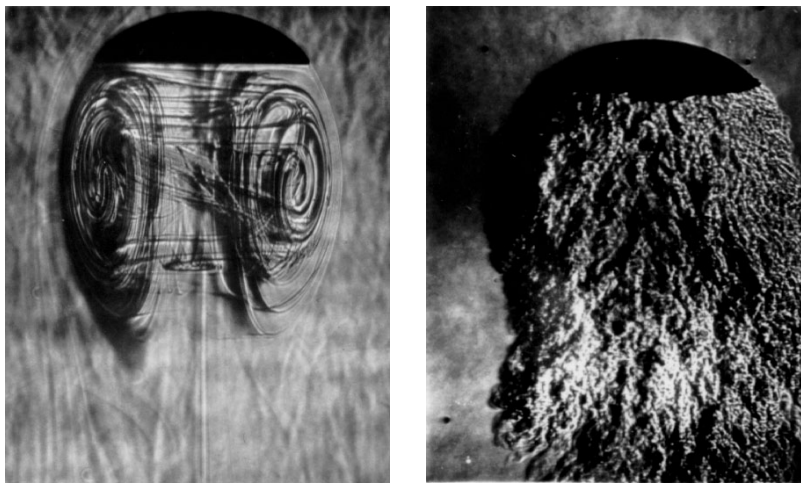


Figure 3: Flow visualizations of spherical-cap bubbles. On the left is a bubble with a laminar wake at $Re \approx 180$ (from Wegener and Parlange 1973) and, on the right, a bubble with a turbulent wake at $Re \approx 17,000$ (from Wegener, Sundell and Parlange 1971, reproduced with permission of the authors).

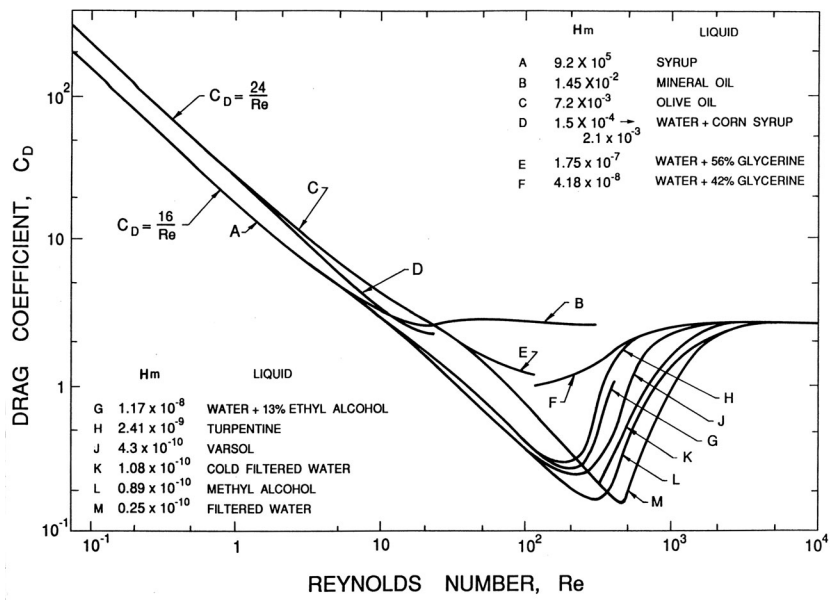


Figure 4: Drag coefficients, C_D , for bubbles as a function of the Reynolds number, Re , for a range of Haberman-Morton numbers, Hm , as shown. Data from Haberman and Morton (1953).